AN2450
Application note

LLC resonant half-bridge converter design guideline

Silvio De Simone

Introduction

The growing popularity of the LLC resonant converter in its half-bridge implementation (see *Figure 1 on page 4*) is due to its high-efficiency, low level of EMI emissions, and its ability to achieve high power density. Such features perfectly fit the power supply demand of many modern applications such as LCD and PDP TV or 80+ initiative compliant ATX silver box. One of the major difficulties that engineers are facing with this topology is the lack of information concerning the way the converter operates and, therefore, the way to design it in order to optimize its features.

The purpose of this application note is to provide a detailed quantitative analysis of the steady state operation of the topology that can be easily translated into a design procedure.

Exact analysis of LLC resonant converters (see *1.* of *Section 9: Reference on page 34*) leads to a complex model that cannot be easily used to derive a handy design procedure. R. L. Steigerwald (see *2.* of *Section 9: Reference*) has described a simplified method, applicable to any resonant topology, based on the assumption that input to output power transfer is essentially due to the fundamental Fourier series components of currents and voltages.

This is what is commonly known as the "first harmonic approximation" (FHA) technique, which enables the analysis of resonant converters by means of classical complex ac circuit analysis. This is the approach that has been used in this paper.

The same methodology has been used by T. Duerbaum (see *3.* of *Section 9*) who has highlighted the peculiarities of this topology stemming from its multi-resonant nature. Although it provides an analysis useful to set up a design procedure, the quantitative aspect is not fully complete since some practical design constraints, especially those related to soft-switching, are not addressed. In (see *4.* of *Section 9*) a design procedure that optimizes transformer's size is given but, again, many other significant aspects of the design are not considered.

The application note starts with a brief summary of the first harmonic approximation approach, giving its limitations and highlighting the aspects it cannot predict. Then, the LLC resonant converter is characterized as a two-port element, considering the input impedance, and the forward transfer characteristic. The analysis of the input impedance is useful to determine a necessary condition for Power MOSFETs' ZVS to occur and allows the designer to predict how conversion efficiency behaves when the load changes from the maximum to the minimum value. The forward transfer characteristic (see *Figure 3 on page 10*) is of great importance to determine the input to output voltage conversion ratio and provides considerable insight into the converter's operation over the entire range of input voltage and output load. In particular, it provides a simple graphical means to find the condition for the converter to regulate the output voltage down to zero load, which is one of the main benefits of the topology as compared to the traditional series resonant converter.

Contents

List of figures

1 FHA circuit model

The FHA approach is based on the assumption that the power transfer from the source to the load through the resonant tank is almost completely associated to the fundamental harmonic of the Fourier expansion of the currents and voltages involved. This is consistent with the selective nature of resonant tank circuits.

Figure 1. LLC resonant half-bridge converter
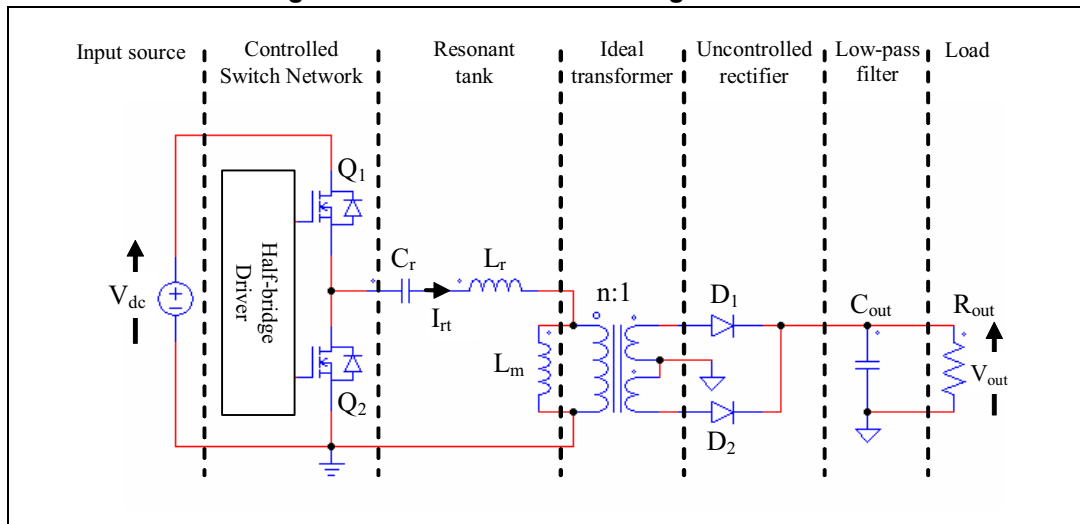
The harmonics of the switching frequency are then neglected and the tank waveforms are assumed to be purely sinusoidal at the fundamental frequency: this approach gives quite accurate results for operating points at and above the resonance frequency of the resonant tank (in the continuous conduction mode), while it is less accurate, but still valid, at frequencies below the resonance (in the discontinuous conduction mode).

It is worth pointing out also that many details of circuit operation on a cycle-to-cycle time base will be lost. In particular, FHA provides only a necessary condition for MOSFETs' zero-voltage switching (ZVS) and does not address secondary rectifiers' natural ability to work always in zero-current switching (ZCS). A sufficient condition for Power MOSFETs' ZVS will be determined in *Section 3: ZVS constraints on page 16* still in the frame of FHA approach.

Let us consider the simple case of ideal components, both active and passive.

The two Power MOSFETs of the half-bridge in *Figure 1* are driven on and off symmetrically with 50% duty cycle and no overlapping. Therefore the input voltage to the resonant tank $v_{sq}(t)$ is a square waveform of amplitude V_{dc}, with an average value of $V_{dc}/2$. In this case the capacitor C_r acts as both resonant and dc blocking capacitor. As a result, the alternate voltage across C_r is superimposed to a dc level equal to $V_{dc}/2$.

The input voltage waveform $v_{sq}(t)$ of the resonant tank in *Figure 1* can be expressed in Fourier series:

Equation 1

$$v_{sq}(t) = \frac{V_{dc}}{2} + \frac{2}{\pi}V_{dc}\sum_{n = 1, 3, 5. \ldots}\frac{1}{n}\sin(n2\pi f_{sw}t)$$

whose fundamental component $v_{i.FHA}(t)$ (in phase with the original square waveform) is:

Equation 2

$$v_{iFHA}(t) = \frac{2}{\pi} V_{dc} \sin(2\pi f_{sw}t)$$

where f_{sw} is the switching frequency. The rms value $V_{i.FHA}$ of the input voltage fundamental component is:

Equation 3

$$v_{iFHA} = \frac{\sqrt{2}}{\pi} V_{dc}$$

As a consequence of the above mentioned assumptions, the resonant tank current $i_{rt}(t)$ will be also sinusoidal, with a certain rms value I_{rt} and a phase shift Φ with respect to the fundamental component of the input voltage:

Equation 4

$$i_{rt}(t) = \sqrt{2}I_{rt}\sin(2\pi f_{sw}t - \Phi) = \sqrt{2}I_{rt}\cos\Phi \bullet \sin(2\pi f_{sw}t) - \sqrt{2}I_{rt}\sin\Phi \bullet \cos(2\pi f_{sw}t)$$

This current lags or leads the voltage, depending on whether inductive reactance or capacitive reactance dominates in the behavior of the resonant tank in the frequency region of interest. Irrespective of that, $i_{rt}(t)$ can be obtained as the sum of two contributes, the first in phase with the voltage, the second with 90° phase-shift with respect to it.

The dc input current $I_{i.dc}$ from the dc source can also be found as the average value, along a complete switching period, of the sinusoidal tank current flowing during the high-side MOSFET conduction time, when the dc input voltage is applied to the resonant tank:

Equation 5

$$I_{idc} = \frac{1}{T_{sw}} \int_0^{\frac{T_{sw}}{2}} i_{rt}(t)dt = \frac{\sqrt{2}}{\pi} I_{rt}\cos\Phi$$

where T_{sw} is the time period at switching frequency.

The real power P_{in}, drawn from the dc input source (equal to the output power P_{out} in this ideal case) can now be calculated as both the product of the input dc voltage V_{dc} times the average input current $I_{i.dc}$ and the product of the rms values of the voltage and current's first harmonic, times $\cos\Phi$:

Equation 6

$$P_{in} = V_{dc}I_{idc} = V_{iFHA}I_{rt}\cos\Phi$$

the two expressions are obviously equivalent.

The expression of the apparent power P_{app} and the reactive power P_r are respectively:

Equation 7

$$P_{app} = V_{iFHA}I_{rt} \qquad\qquad P_r = V_{iFHA}I_{rt}\sin\Phi$$

Let us consider now the output rectifiers and filter part. In the real circuit, the rectifiers are driven by a quasi-sinusoidal current and the voltage reverses when this current becomes zero; therefore the voltage at the input of the rectifier block is an alternate square wave in phase with the rectifier current of amplitude V_{out}.

The expressions of the square wave output voltage $v_{o.sq}(t)$ is:

Equation 8

$$V_{osq}(t) = \frac{4}{\pi} V_{out} \sum_{n = 1, 3, 5...} \frac{1}{n} \sin(n2\pi f_{sw}t - \Psi)$$

which has a fundamental component $v_{o.FHA}(t)$:

Equation 9

$$V_{oFHT}(t) = \frac{4}{\pi} V_{out} \sin(2\pi f_{sw}t - \Psi)$$

whose rms amplitude is:

Equation 10

$$V_{oFHA} = \frac{2\sqrt{2}}{\pi} V_{out}$$

where Ψ is the phase shift with respect to the input voltage. The fundamental component of the rectifier current $_{irect}(t)$ will be:

Equation 11

$$i_{rect}(t) = \sqrt{2} I_{rect} \sin(2\pi f_{sw}t - \Psi)$$

where I_{rect} is its rms value.

Also in this case we can relate the average output current to the load I_{out} and also derive the ac current $I_{c.ac}$ flowing into the filtering output capacitor:

Equation 12

$$I_{out} = \frac{2}{T_{sw}} \int_0^{\frac{T_{sw}}{2}} |i_{rect}(t)| dt = \frac{2\sqrt{2}}{\pi} I_{rect} = \frac{P_{out}}{V_{out}} = \frac{V_{out}}{R_{out}}$$

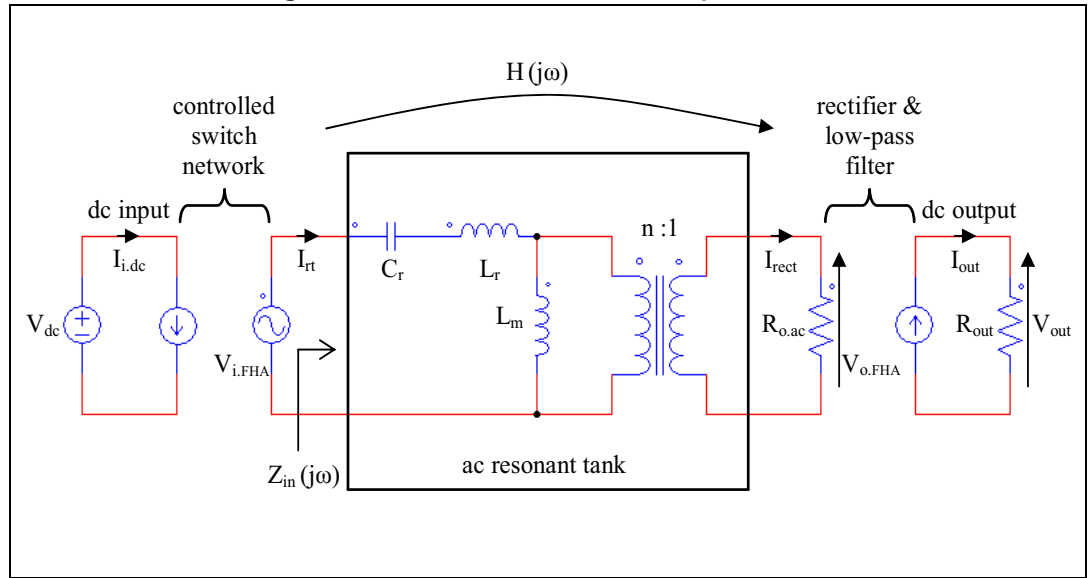**Equation 13**

$$I_{cac} = \sqrt{I_{rect}^2 - I_{out}^2}$$

where P_{out} is the output power associated to the output load resistance R_{out}.

Since $v_{o.FHA}(t)$ and $i_{rect}(t)$ are in phase, the rectifier block presents an effective resistive load to the resonant tank circuit, $R_{o.ac}$, equal to the ratio of the instantaneous voltage and current:

Equation 14

$$R_{oac} = \frac{v_{o.FHA}(t)}{i_{rect}(t)} = \frac{V_{o.FHA}}{I_{rect}} = \frac{8}{\pi^2}\frac{V_{out}^2}{P_{out}} = \frac{8}{\pi^2}R_{out}$$

Thus, in the end, we have transformed the non linear circuit of *Figure 1* into the linear circuit of *Figure 2*, where the ac resonant tank is excited by an effective sinusoidal input source and drives an effective resistive load. This transformation allows the use of complex ac-analysis methods to study the circuit and, furthermore, to pass from ac to dc parameters (voltages and currents), since the relationships between them are well-defined and fixed (see *Equation 3*, *Equation 5*, *Equation 6*, *Equation 10* and *Equation 12* above).

Figure 2. FHA resonant circuit two port model

The ac resonant tank in the two-port model of *Figure 2* can be defined by its forward transfer function H(s) and input impedance $Z_{in}(s)$:

Equation 15

$$H(s) = \frac{V_{oFHA}(s)}{V_{iFHA}(s)} = \frac{1}{n}\frac{n^2 R_{oac} \parallel sL_m}{Z_{in}(s)}$$

Equation 16

$$Z_{in}(s) = \frac{V_{iFHA}(s)}{I_{rt}(s)} = \frac{1}{sC_r} + sL_r + n^2 R_{oac} \parallel sL_m$$

For the discussion that follows it is convenient to define the effective resistive load reflected to the primary side of the transformer R_{ac}:

Equation 17

$$R_{ac} = n^2 R_{oac}$$

And the so-called "normalized voltage conversion ratio" or "voltage gain" $M(f_{sw})$:

Equation 18

$$M(f_{sw}) = n\|H(j2\pi f_{sw})\| = n\frac{V_{oFHA}}{V_{iFHA}}$$

It can be demonstrated (by applying the relationships of *Equation 3*, *Equation 10* and *Equation 18* to the circuit in *Figure 2*) that the input to output dc-dc voltage conversion ratio is equal to:

Equation 19

$$\frac{V_{out}}{V_{dc}} = \frac{1}{2n}M(f_{sw})$$

In other words, the voltage conversion ratio is equal to one half the module of resonant tank's forward transfer function evaluated at the switching frequency.

2 Voltage gain and input impedance

Starting from *Equation 18* we can obtain the expression of the voltage gain:

Equation 20

$$M(f_n, \lambda, Q) = \frac{1}{\sqrt{\left(1 + \lambda - \dfrac{\lambda}{f_n^2}\right)^2 + Q^2\left(f_n - \dfrac{1}{f_n}\right)^2}}$$

with the following parameter definitions:

resonance frequency: $f_r = \dfrac{1}{2\pi\sqrt{L_r C_r}}$

characteristic impedance: $Z_o = \sqrt{\dfrac{L_r}{C_r}} = 2\pi f_r L_r = \dfrac{1}{2\pi f_r C_r}$

quality factor: $Q = \dfrac{Z_o}{R_{ac}} = \dfrac{Z_o}{n^2 R_{oac}} = \dfrac{\pi^2}{8}\dfrac{Z_0}{n^2}\dfrac{P_{out}}{V_{out}^2}$

inductance ratio: $\lambda = \dfrac{L_r}{L_m}$

normalized frequency: $f_n = \dfrac{f_{sw}}{f_r}$

Under no-load conditions, (i.e. Q = 0) the voltage gain assumes the following form:

Equation 21

$$M_{OL}(f_n, \lambda) = \frac{1}{\left|1 + \lambda - \dfrac{\lambda}{f_n^2}\right|}$$

Figure 3 shows a family of plots of the voltage gain versus normalized frequency. For different values of Q, with λ = 0.2, it is clearly visible that the LLC resonant converter presents a load-independent operating point at the resonance frequency f_r (f_n = 1), with unity gain, where all the curves are tangent (and the tangent line has a slope -2λ). Fortunately, this load-independent point occurs in the inductive region of the voltage gain characteristic, where the resonant tank current lags the input voltage square waveform (which is a necessary condition for ZVS behavior).

The regulation of the converter output voltage is achieved by changing the switching frequency of the square waveform at the input of the resonant tank: since the working region is in the inductive part of the voltage gain characteristic, the frequency control circuit that keeps the output voltage regulated acts by increasing the frequency in response to a decrease of the output power demand or to an increase of the input dc voltage. Considering this, the output voltage can be regulated against wide loads variations with a relatively narrow switching frequency change, if the converter is operated close to the load-independent point. Looking at the curves in *Figure 3*, it is obvious that the wider the input dc voltage range is, the wider the operating frequency range will be, in which case it is difficult

to optimize the circuit. This is one of the main drawbacks common to all resonant topologies.

This is not the case, however, when there is a PFC pre-regulator in front of the LLC converter, even with a universal input mains voltage (85 V_{ac} - 264 V_{ac}). In this case, in fact, the input voltage of the resonant converter is a regulated high voltage bus of ~400 V_{dc} nominal, with narrow variations in normal operation, while the minimum and maximum operating voltages will depend, respectively, on the PFC pre-regulator hold-up capability during mains dips and on the threshold level of its overvoltage protection circuit (about 10 - 15% over the nominal value). Therefore, the resonant converter can be optimized to operate at the load-independent point when the input voltage is at nominal value, leaving to the step-up capability of the resonant tank (i.e. operation below resonance) the handling of the minimum input voltage during mains dips.

Figure 3. Conversion ratio of LLC resonant half-bridge
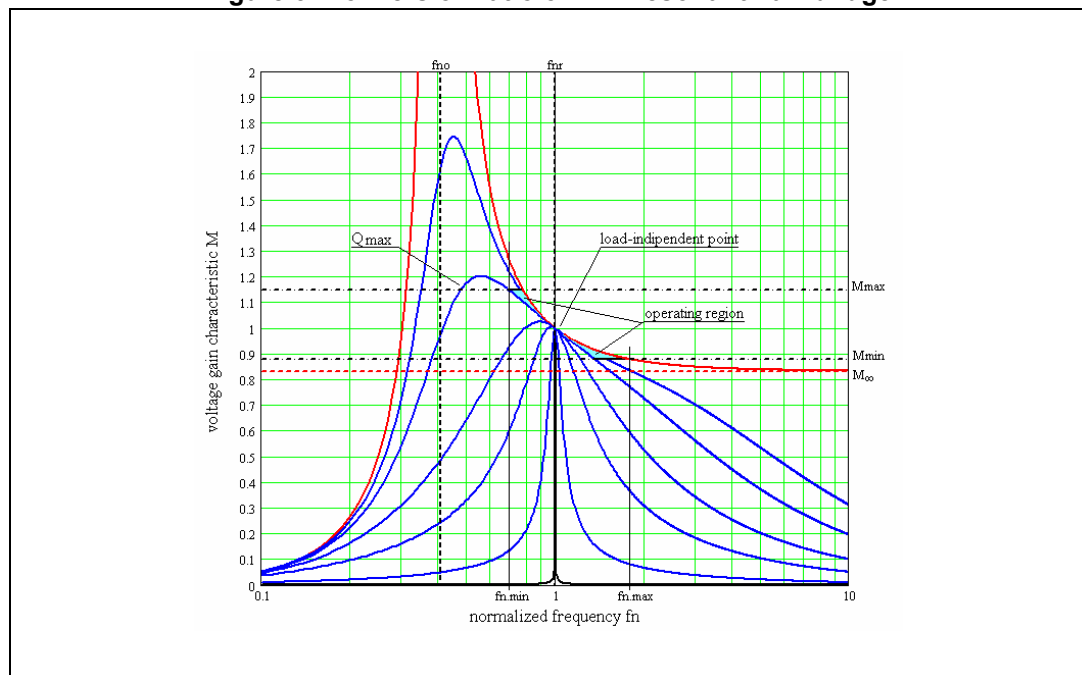
The red curve in *Figure 3* represents the no-load voltage gain curve M_{OL}; for normalized frequency going to infinity, it tends to an asymptotic value M_∞:

Equation 22

$$M_\infty = M_{OL}(f_n \rightarrow \infty, \lambda) = \frac{1}{1+\lambda}$$

Moreover, a second resonance frequency f_o can be found, which refers to the no-load condition or when the secondary side diodes are not conducting (i.e. the condition where the total primary inductance $L_r + L_m$ resonates with the capacitor C_r); f_o is defined as:

Equation 23

$$f_o = \frac{1}{2\pi\sqrt{(L_r + L_m)C_r}} = f_r\sqrt{\frac{\lambda}{1+\lambda}}$$

or in normalized form:

Equation 24

$$f_{no} = \frac{f_o}{f_r} = \sqrt{\frac{\lambda}{1+\lambda}}$$

At this frequency the no-load gain curve M_{OL} tends to infinity.

By imposing that the minimum required gain M_{min} (at max. input dc voltage) is greater than the asymptotic value M_∞, it is possible to ensure that the converter can work down to no-load at a finite operating frequency (which will be the maximum operating frequency of the converter):

Equation 25

$$M_{min} = 2n\frac{V_{out}}{V_{dcmax}} > \frac{1}{1+\lambda}$$

The maximum required gain M_{max} (at min. input dc voltage) at max. output load (max. P_{out}), that is at max. Q, will define the min. operating frequency of the converter:

Equation 26

$$M_{max} = 2n\frac{V_{out}}{V_{dcmin}}$$

Given the input voltage range ($V_{dc.min}$ - $V_{dc.max}$), three types of operations are possible:
* always below resonance frequency (step-up operations)
* always above resonance frequency (step-down operations)
* across the resonance frequency (shown in *Figure 3*).

Looking at *Figure 4*, we can see that an increase of the inductance ratio value λ has the effect of shrinking the gain curves in the M - f_n plane toward the resonance frequency f_{nr} (which means the no-load resonance frequency f_{no} increases) and contemporaneously reduces the asymptotic level M_∞ of the no-load gain characteristic. At the same time the peak gain of each curve increases.

Figure 4. Shrinking effect of λ value increase
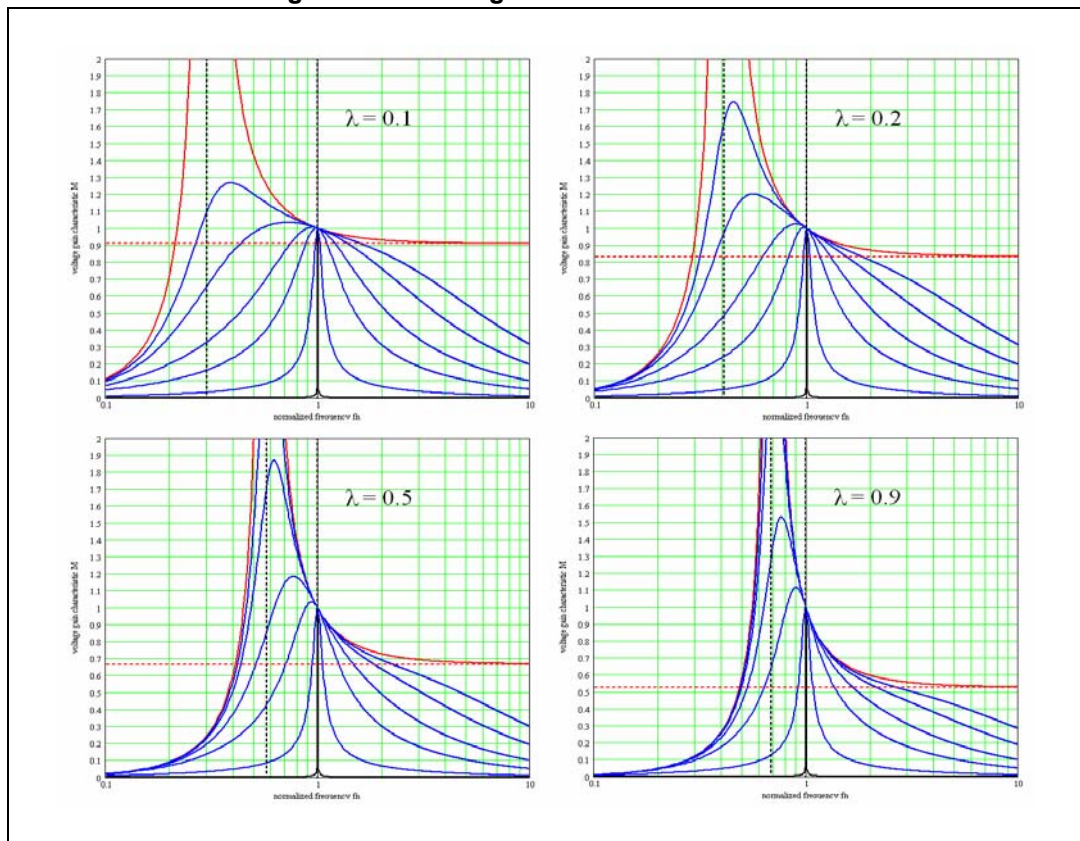
Starting from *Equation 16 on page 7* we can obtain the expression of the normalized input impedance Z_n of the resonant tank:

Equation 27

$$Z_n(f_n, \lambda, Q) = \frac{Z_{in}(f_n, \lambda, Q)}{Z_o} = \frac{jf_n}{\lambda + jf_nQ} + \frac{1 - f_n^2}{jf_n}$$

whose magnitude is plotted in *Figure 5*, at different Q values, with $\lambda = 0.2$.

The red and blue curves in the above mentioned figure represent the no-load and short-circuit cases respectively, and are characterized by asymptotes at the two normalized resonance frequencies f_{no} and f_{nr} (= 1). All the curves at different values of Q intercept at normalized frequency $f_{n.cross}$:

Equation 28

$$f_{n.cross} = \sqrt{\frac{2\lambda}{1 + 2\lambda}}$$

At frequencies higher than the crossing frequency $f_{n.cross}$, the input impedance behaves such that at increasing output current I_{out} (that is at increasing P_{out} and Q) it decreases (coherently to the load resistance); the opposite happens at frequencies lower than $f_{n.cross}$, where the input impedance increases, while the output load resistance decreases.

Figure 5. Normalized input impedance magnitude
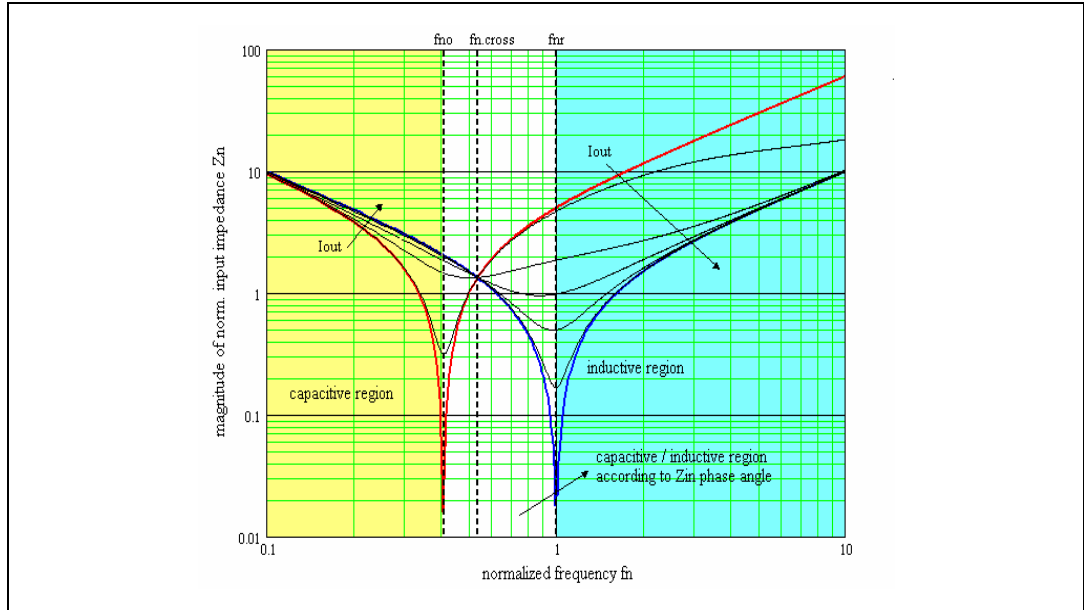
The ac analysis can also help to estimate converter's efficiency η and predict how this changes with the load. Considering the generic model similar to the one in *Figure 2 on page 7*, where the resonant tank includes also the dissipative elements (i.e. series resistors for magnetic components winding losses and capacitor's ESR, and parallel resistors for magnetic losses of inductors and transformer), we can compute the transfer function $H_{LOSS}(j\omega)$ and the input impedance $Z_{in.LOSS}(j\omega)$. By calculating input and output power in terms of H_{LOSS} and $Z_{in.LOSS}$, we get:

Equation 29

$$\eta = \frac{P_{out}}{P_{in}} = \frac{\|H_{LOSS}(j\omega)\|^2}{R_{oac}Re[Y_{inLOSS}(j\omega)]}$$

where $Y_{in.LOSS}$ is the admittance (reciprocal of $Z_{in.LOSS}$) and the input and output power are expressed as:

Equation 30

$$P_{in} = V_{iFHA}I_{rt}\cos\Phi = V_{iFHA}{}^2 Re\left[\frac{1}{Z_{inLOSS}(j\omega)}\right]$$

Equation 31

$$P_{out} = V_{o\cdot FHA}I_{rect} = \frac{V^2_{o\cdot FHA}}{R_{o\cdot ac}} = \frac{V^2_{iFHA}}{R_{o\cdot ac}} \cdot \|H_{LOSS}(j\omega)\|^2$$

The region on the left-hand side of the diagram in *Figure 5*, i.e. for a normalized frequency lower than f_{no}, is the capacitive region, where the tank current leads the half-bridge square voltage; at normalized frequency higher than the resonance frequency f_{nr} (= 1), on the right-hand side region, the input impedance is inductive, and the resonant tank current lags the input voltage. In the region between the two resonance frequencies the impedance can be either capacitive or inductive, depending on the value of the impedance phase angle.

By imposing that the imaginary part of $Z_n(f_n, \lambda, Q)$ is zero (which means imposing that Z_{in} has zero phase angle, as Z_o is real and does not affect the phase), we can find the boundary condition between capacitive and inductive mode operation of the LLC resonant converter.

The analytical results are the following:

Equation 32

$$f_{nZ}(\lambda, Q) = \sqrt{\frac{Q^2 - \lambda(1 + \lambda) + \sqrt{[Q^2 - \lambda(1 + \lambda)]^2 + 4Q^2\lambda^2}}{2Q^2}}$$

Equation 33

$$Q_Z(f_n, \lambda) = \sqrt{\frac{\lambda}{1 - f_n^2} - \left(\frac{\lambda}{f_n}\right)^2}$$

where f_{nZ} represents the normalized frequency where, for a fixed couple (λ- Q), the input resonant tank impedance is real (and only real power is absorbed from the source); while Q_Z is the maximum value of the quality factor, below which, at a fixed normalized frequency and inductance ratio (f_n - λ) the tank impedance is inductive; hence, the maximum voltage gain available in that condition is also found:

Equation 34

$$M_{MAX}(\lambda, Q) = M(f_{nZ}(\lambda, Q), \lambda, Q)$$

By plotting the locus of operating points $[M_{MAX}(\lambda, Q), f_{nZ}(\lambda, Q)]$, whose equation on M - f_n plane is the following:

Equation 35

$$M_Z(f_n, \lambda) = \frac{f_n}{\sqrt{f_n^2(1 + \lambda) - \lambda}}$$

we can draw the borderline between capacitive and inductive mode in the region between the two resonance frequencies, shown in *Figure 6*. It is also evident that the peak value of the gain characteristics for a given quality factor Q value, already lies in the capacitive region.

Figure 6. Capacitive and inductive regions in M - f_n plane
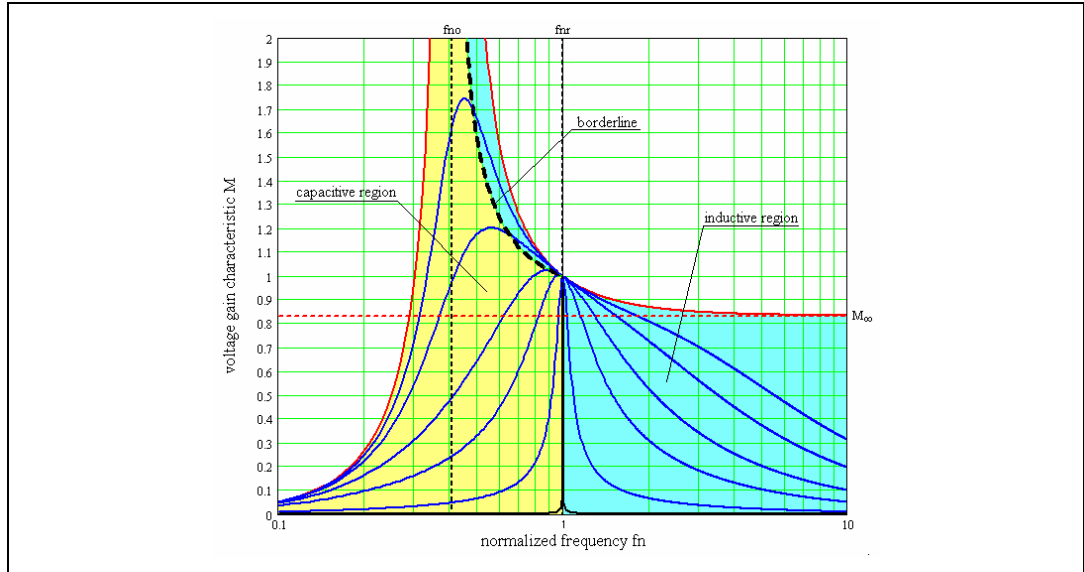
Moreover, by equating the second term of (*Equation 35*) to the maximum required gain M_{max} (at minimum input voltage), and solving for f_n, we get the minimum operating frequency $f_{n.min}$ which allows the required maximum voltage gain at the boundary between capacitive and inductive mode:

Equation 36

$$f_{nmin} = \sqrt{\dfrac{1}{1 + \dfrac{1}{\lambda}\left(1 - \dfrac{1}{M_{max}^2}\right)}}$$

Furthermore, by substituting the minimum frequency (*Equation 36*) into the *Equation 33*, we get the maximum quality factor Q_{max} which allows the required maximum voltage gain at the boundary between capacitive and inductive mode:

Equation 37

$$Q_{max} = \dfrac{\lambda}{M_{max}}\sqrt{\dfrac{1}{\lambda} + \dfrac{M_{max}^2}{M_{max}^2 - 1}}$$

Finally, by equating the second term of the no-load transfer function (*Equation 21 on page 9*) to the minimum required voltage gain M_{min}, it is possible to find the expression of the maximum normalized frequency $f_{n.max}$:

Equation 38

$$f_{nmax} = \sqrt{\dfrac{1}{1 + \dfrac{1}{\lambda}\left(1 - \dfrac{1}{M_{min}}\right)}}$$

3 ZVS constraints

The assumption that the working region lies inside the inductive region of operation is only a necessary condition for the ZVS of the half-bridge MOSFETs, but not sufficient; this is because the parasitic capacitance of the half-bridge midpoint, neglected in the FHA analysis, needs energy to be charged and depleted during transitions. In order to understand ZVS behavior, refer to the half-bridge circuit in *Figure 7*, where the capacitors C_{oss} and C_{stray} are, respectively, the effective drain-source capacitance of the Power MOSFETs and the total stray capacitance present across the resonant tank impedance, so that the total capacitance C_{zvs} at node N is:

Equation 39

$$C_{zvs} = 2C_{OSS} + C_{stray}$$

which, during transitions, swings by $\Delta V = V_{dc}$. To allow ZVS, the MOSFET driving circuit is such that a dead time T_D is inserted between the end of the ON-time of either MOSFET and the beginning of the ON-time of the other one, so that both are not conducting during T_D.

Figure 7. Circuit behavior at ZVS transition
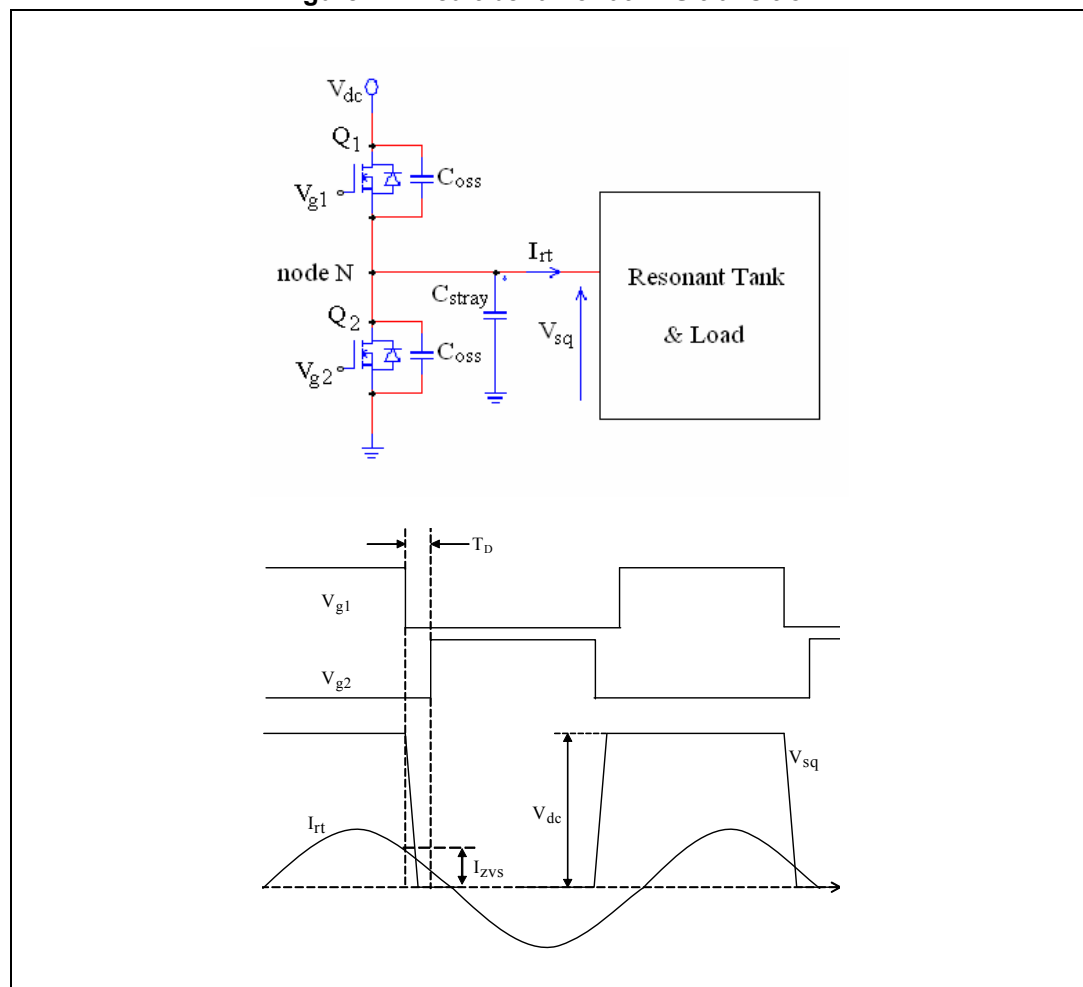
Due to the phase lag of the input current with respect to the input voltage, at the end of the first half cycle the inductor current I_{rt} is still flowing into the circuit and, therefore it can deplete C_{ZVS} so that its voltage swings from ΔV to zero (it will be vice versa during the second half cycle).

In order to guarantee ZVS, the tank current at the end of the first half cycle (considering the dead time negligible as compared to the switching period, so that the current change is negligible as well) must exceed the minimum value necessary to deplete C_{ZVS} within the dead time interval T_D, which means:

Equation 40

$$I_{zvs} = i_{rt}\left(\frac{T_{sw}}{2}\right) = C_{zvs}\frac{\Delta V}{T_D} = (2C_{OSS} + C_{stray})\frac{V_{dc}}{T_D}$$

This current equals, of course, the peak value of the reactive current flowing through the resonant tank (it is 90° out-of-phase); the one that determines the reactive power level into the circuit:

Equation 41

$$I_{zvs} = \sqrt{2}I_{rt}\sin\Phi$$

Moreover, as the rms component of the tank current associated to the active power is:

Equation 42

$$I_{act} = I_{rt}\cos\Phi = \frac{P_{in}}{V_{iFHA}}$$

we can derive also the rms value of the resonant tank current and the phase lag Φ between input voltage and current (that is the input impedance phase angle at that operating point):

Equation 43

$$I_{rt} = \sqrt{I_{rt}^2\cos(\Phi)^2 + I_{rt}^2\sin(\Phi)^2} = \sqrt{\left(\frac{P_{in}}{V_{iFHA}}\right)^2 + \frac{I_{zvs}^2}{2}}$$

Equation 44

$$\Phi = a\cos\left(\frac{P_{in}}{V_{iFHA}I_{rt}}\right)$$

Thus we can write the following analytic expression:

Equation 45

$$\tan(\Phi) = \frac{Im[Z_n(f_n, \lambda, Q)]}{Re[Z_n(f_n, \lambda, Q)]} \geq \frac{C_{zvs}}{\pi T_D}\frac{V_{dc}^2}{P_{in}}$$

which is the sufficient condition for ZVS of the half-bridge Power MOSFETs, to be applied to the whole operating range. The solution of *Equation 45* for the quality factor Q_{zvs} that ensures ZVS behavior at full load and minimum input voltage is not convenient.

Therefore, we can calculate the Q_{max} value (at max. output power and min. input voltage), where the input impedance has zero phase, and take some margin (5% - 10%) by choosing:

Equation 46

$$Q_{zvs.1} = 90\% \div 95\% \bullet Q_{max}$$

and check that the condition (*Equation 45*) is satisfied at the end of the process, once the resonant tank has been completely defined. The process will be iterated if necessary.

Of course the sufficient condition for ZVS needs to be satisfied also at no-load and maximum input voltage; in this operating condition it is still possible to find an additional constraint on the maximum quality factor at full load to guarantee ZVS. In fact the input impedance at no-load $Z_{in.OL}$ has the following expression:

Equation 47

$$Z_{in.OL}(f_n) = jZ_o\left[f_n\left(1+\frac{1}{\lambda}\right)-\frac{1}{f_n}\right]$$

Taking into account that:

Equation 48

$$Z_o = R_{ac}Q$$

and writing the sufficient condition for ZVS in this operating condition, that is:

Equation 49

$$\frac{V_{iFHAmax}}{\|Z_{inOL}(f_{n.max})\|} \geq \frac{I_{zvs(Vdcmax)}}{\sqrt{2}}$$

we get the constraint on the quality factor for the ZVS at no-load and maximum input voltage:

Equation 50

$$Q_{zvs2} \leq \frac{2}{\pi}\frac{\lambda f_{nmax}}{(\lambda+1)f_{nmax}^2-\lambda}\frac{T_D}{R_{ac}C_{zvs}}$$

Therefore, in order to guarantee ZVS over the whole operating range of the resonant converter, we have to choose a maximum quality factor value lower than the smaller of $Q_{zvs.1}$ and $Q_{zvs.2}$.

4   Operation under overload and short-circuit condition

An important aspect to analyze is the converter's behavior during output overload and/or short-circuit.

Referring to the voltage gain characteristics in *Figure 8*, let us suppose that the resonant tank has been designed to operate in the inductive region for a maximum output power $P_{out.max}$ (corresponding to the curve $Q = Q_{max}$) at a given output-to-input voltage ratio (corresponding to the horizontal line $M = M_x$) greater than 1.

When the output power is increased from zero to the maximum value, the gain characteristic relative to each power level changes progressively from the red curve ($Q = 0$) to the black one (Q_{max}). The control loop keeps the value of M equal to M_x, then the quiescent point moves along the horizontal line $M = M_x$ and the operating frequency at each load condition is given by the abscissa of the crossover between the horizontal line $M = M_x$ and the voltage gain characteristic relevant to the associated value of Q.

Figure 8. Voltage gain characteristics of the LLC resonant tank
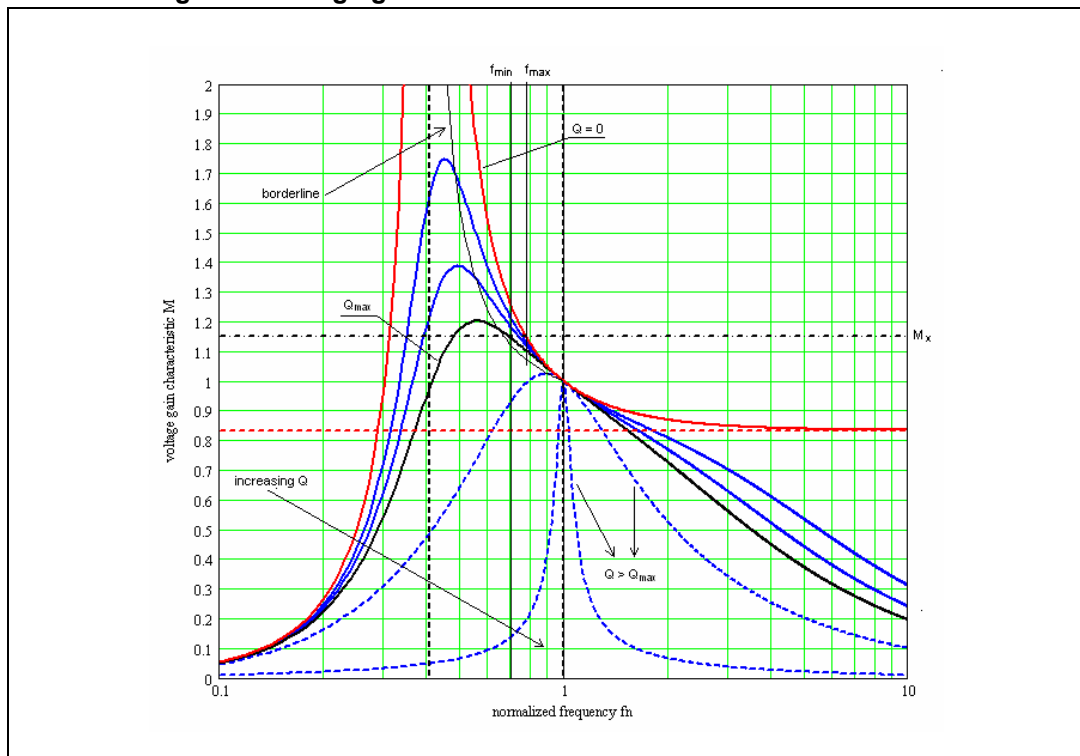
If the load is increased over the maximum specified (associated to the curve $Q = Q_{max}$) eventually the converter's operating point will invariably enter the capacitive region, where hard switching of Power MOSFETs may cause device failures, if no corrective action is taken.

In fact, for values of Q sufficiently greater than Q_{max} the intersection with the $M = M_x$ line will take place on the left-hand side of the borderline curve and, then, in the capacitive region; moreover, if Q exceeds the value corresponding to the characteristic curve tangent to $M = M_x$ there will no longer be a possible operating point with $M = M_x$. This means that the

converter will no longer be able to keep the output voltage regulated and the output voltage will fall despite the reduction of the operating frequency (feedback reversal).

Limiting the minimum operating frequency (e.g. at the frequency value corresponding to the intersection of $M = M_x$ with $Q = Q_{max}$) is not enough to prevent the converter from entering the capacitive region of operation. In fact, as the minimum frequency is reached, from that point onwards a further load increase will make the operating point move along the vertical line $f = f_{min}$ and eventually cross the borderline.

Limiting the minimum operating frequency is effective in preventing capacitive mode operation only if the minimum (normalized) frequency value is greater than 1. This suggests that, in response to an overload/short-circuit condition at the output, the converter operating frequency must be pushed above the resonance frequency (it is better if well above it) in order to decrease power throughput.

It is worth noticing that, if the converter is specified to deliver a peak output power (where output voltage regulation is to be maintained) greater than the maximum continuous output power for a limited time, the resonant tank must be designed for peak output power to make sure that it will not run in capacitive mode. Of course, its thermal design will consider only the maximum continuous power.

In any case, whatever the converter specified, short-circuit conditions or, in general, overload conditions exceeding the maximum specified for the tank circuit, need to be handled with additional means, such as a current limitation circuit.

5 Magnetic integration

The LLC resonant half-bridge is well suited for magnetic integration, i.e. to combine the inductors as well as the transformer into a single magnetic device. This can be easily recognized looking at the transformer's physical model in *Figure 9*, where the topological analogy with the inductive part of the LLC tank circuit is apparent. However, the real transformer has leakage inductance on the secondary side as well, which is completely absent in the model considered so far. To include the effect of secondary leakage in the FHA analysis, we need a particular transformer model and a simplifying assumption.

It is well known that there are an infinite number of electrically equivalent models of a given transformer, depending on the choice of the turn ratio of the ideal transformer included in the model. With an appropriate choice of this "equivalent" turn ratio n (obviously different from the "physical" turn ratio n_t = N1/N2) all the elements related to leakage flux can be located on the primary side.

This is the APR (all primary referred) model shown in *Figure 10*, which fits the circuit considered in the FHA analysis. It is possible to show that the APR model is obtained with the following choice of *n*:

Equation 51

$$n = k\sqrt{\frac{L_1}{L_2}}$$

with *k* transformer's coupling coefficient, L_1 inductance of the primary winding and L_2 inductance of each secondary winding. Note that L_r still has physical meaning: it is the primary inductance measured with the secondary windings shorted. Note also that the primary inductance L_1 must be unchanged. It is only differently split in the 2 models of *Figure 9* and *Figure 10*, hence, L_m will be the difference between L_1 and L_r.

In the end, the analysis done so far is directly applicable to real-world transformers provided they are represented by their equivalent APR model. Vice versa, a design flow based on the FHA analysis will provide the parameters of the APR model; hence, an additional step is needed to determine those of the physical model. In particular this applies to the turn number n_t, since L_r and L_m still have a connection with the physical world ($L_r + L_m = L_{L1} + L_\mu = L_1$).

Figure 9. Transformer's physical model
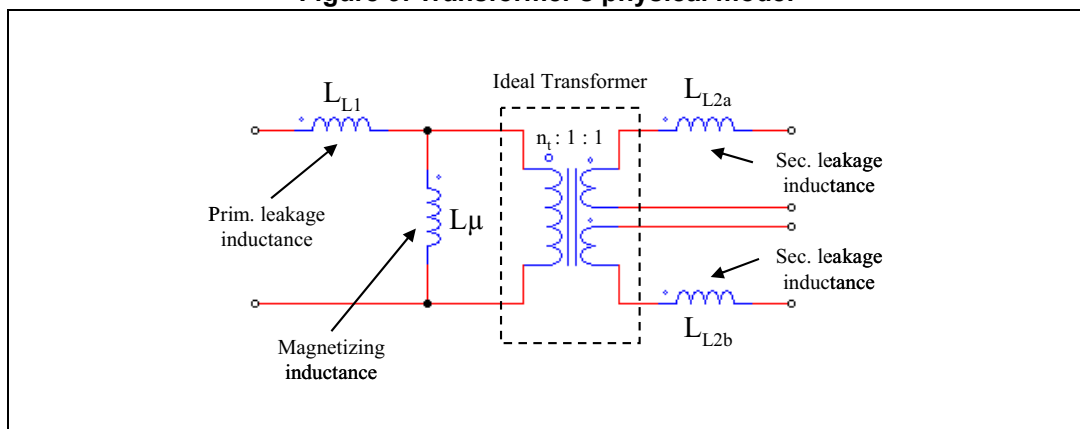
Figure 10. Transformer's APR (all primary referred) model
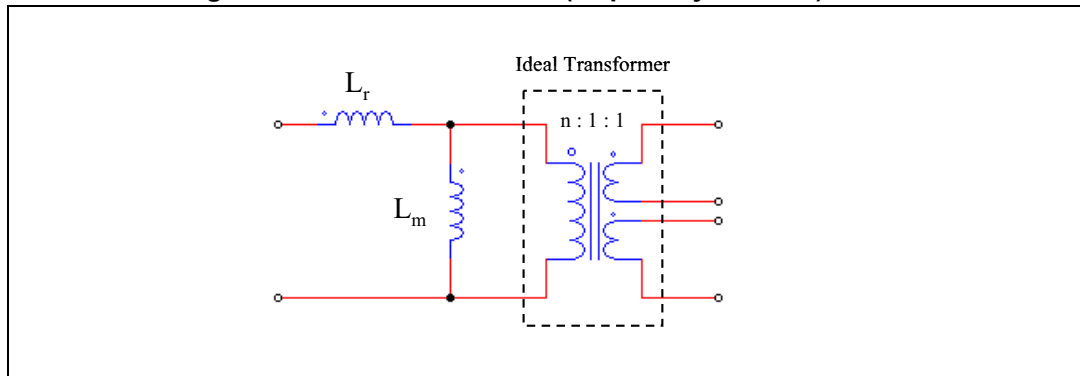
The problem is mathematically undetermined: there are 5 unknowns (L_{L1}, L_μ, n_t, and L_{L2a}, L_{L2b}) in the physical model and only three parameters in the APR model. The simplifying assumption that overcomes this issue is that of magnetic circuit symmetry: flux linkage is assumed to be exactly the same for both primary and secondary windings. This provides the two missing conditions:

Equation 52

$$L_{L2a} = L_{L2b} = \frac{L_{L1}}{n_t^2}$$

With this assumption it is now possible to find the relationship between n and n_t:

Equation 53

$$n_t = n\sqrt{\frac{L_m + L_r}{L_m}} = n\sqrt{1 + \lambda}$$

Figure 11. Transformer construction: E-cores and slotted bobbin
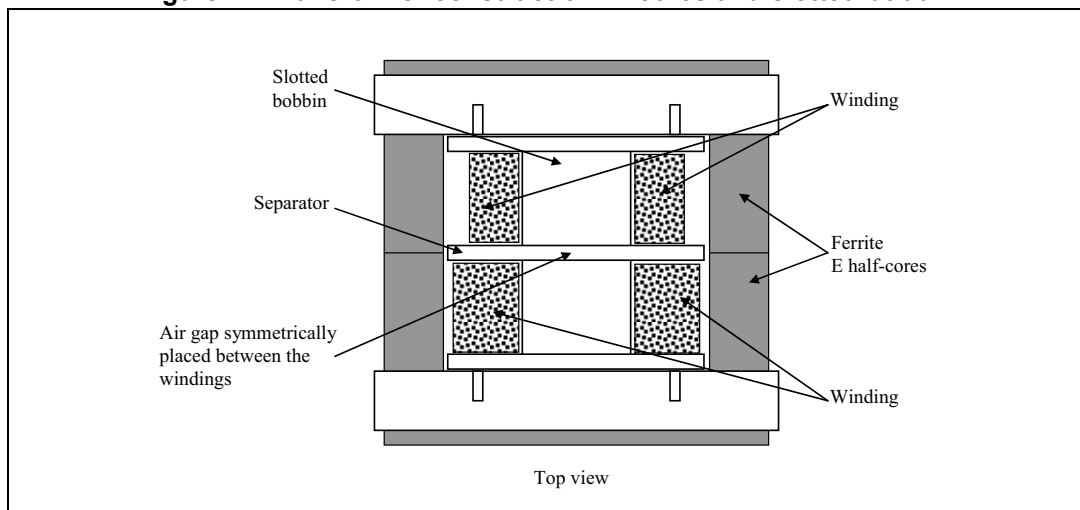
It is not difficult to find real-world structures where the condition of magnetic symmetry is quite close to reality. Consider for example the ferrite E-core plus slotted bobbin assembly, using side-by-side winding arrangement, shown in *Figure 11*.

6 Design procedure

Based on the analysis presented so far, a step-by-step design procedure of an LLC resonant converter is now proposed, which fulfills the following design specification and requires the additional information listed below:

- Design specification:
    - Input voltage range: $V_{dc.min}$ - $V_{dc.max}$
    - Nominal input voltage: $V_{dc.nom}$
    - Regulated output voltage: V_{out}
    - Maximum output power: P_{out}
    - Resonant frequency: f_r
    - Maximum operating frequency: f_{max}
- Additional info:
    - Parasitic capacitance at node N: C_{zvs}
    - Dead time of driving circuit: T_D
- General criteria for the design:
    - The converter will be designed to work at resonance at nominal input voltage.
    - The converter must be able to regulate down to zero load at maximum input voltage.
    - The converter will always work in ZVS in the whole operating range.
- 10 step procedure:
    - Step 1 - to fulfill the first criterion, impose that the required gain at nominal input voltage equals unity and calculate the transformer turn ratio:

Equation 54

$$M_{nom} = 2n\frac{V_{out}}{V_{dc.nom}} = 1 \qquad \Rightarrow \qquad n = \frac{1}{2}\frac{V_{dc.nom}}{V_{out}}$$

- Step 2 - calculate the max. and min. required gain at the extreme values of the input voltage range:

Equation 55

$$M_{max} = 2n\frac{V_{out}}{V_{dc.min}}$$

Equation 56

$$M_{min} = 2n\frac{V_{out}}{V_{dc.max}}$$

–   Step 3 - calculate the maximum normalized operating frequency (according to the definition):

Equation 57

$$f_{n,max} = \frac{f_{max}}{f_r}$$

–   Step 4 - calculate the effective load resistance reflected at transformer primary side, from *Equation 14 on page 7* and *Equation 17 on page 7*:

Equation 58

$$R_{ac} = \frac{8}{\pi^2}n^2\frac{V_{out}^2}{P_{out}}$$

–   Step 5 - impose that the converter operates at maximum frequency at zero load and maximum input voltage, calculating the inductance ratio from *Equation 38 on page 15*:

Equation 59

$$\lambda = \frac{1 - M_{min}}{M_{min}}\frac{f_{nmax}^2}{f_{nmax}^2 - 1}$$

–   Step 6 - calculate the max Q value to work in the ZVS operating region at minimum input voltage and full load condition, from *Equation 37 on page 15* and *Equation 46 on page 18*:

Equation 60

$$Q_{zvs1} = 95\% \bullet Q_{max} = 95\% \bullet \frac{\lambda}{M_{max}}\sqrt{\frac{1}{\lambda} + \frac{M_{max}^2}{M_{max}^2 - 1}}$$

–   Step 7 - calculate the max Q value to work in the ZVS operating region at no-load condition and maximum input voltage, applying *Equation 50 on page 18*:

Equation 61

$$Q_{zvs2} = \frac{2}{\pi}\frac{\lambda f_{nmax}}{(\lambda + 1)f_{nmax}^2 - \lambda}\frac{T_D}{R_{ac}C_{zvs}}$$

–   Step 8 - choose the max quality factor for ZVS in the whole operating range, such that:

Equation 62

$$Q_{zvs} \leq \min\{Q_{zvs1}, Q_{zvs2}\}$$

– Step 9 - calculate the minimum operating frequency at full load and minimum input voltage, according to the following approximate formula:

Equation 63

$$f_{min} = f_r \sqrt{\cfrac{1}{1 + \cfrac{1}{\lambda}\left(1 - \cfrac{1}{\cfrac{1 + \left(\cfrac{Q_{zvs}}{Q_{max}}\right)^4}{M_{max}}}\right)}}$$

– Step 10 - calculate the characteristic impedance of the resonant tank and all component values (from definition):

Equation 64

$$Z_o = Q_{zvs}R_{ac} \qquad C_r = \frac{1}{2\pi f_r Z_o} \qquad L_r = \frac{Z_o}{2\pi f_r} \qquad L_m = \frac{L_r}{\lambda}$$

7 Design example

Here below, a design example follows for a 400 W resonant converter intended to be operated with a front-end PFC with a typical regulated bus voltage of about 400 V.

The STMicroelectronics® resonant controller L6599 is particularly suitable for this application. In fact it incorporates the necessary functions to properly drive the two half-bridge MOSFETs by a 50 percent fixed duty cycle with a fixed dead-time T_D, (between high-side and low-side MOSFET driving signals), changing the frequency according to the feedback signal in order to regulate the output voltages against load and input voltage variations. The main features of the L6599 are a non linear soft-start, a new current protection mode allowing to program the hiccup mode timing, a dedicated pin for sequencing or brown-out (pin LINE) and a standby pin (pin STBY) allowing for the burst mode operation at light load.

The converter specification data are the following:

– Nominal input DC voltage: 390 V

– Input DC voltage range: from 320 to 420 V

– Output voltages: 200 V at 1.6 A continuous current - 75 V at 1.0 A continuous current

– Resonance frequency: 120 kHz

– Max operating frequency: 150 kHz

– Delay time (L6599 datasheet): 270 ns

– Foreseen half-bridge total stray capacitance (at node N): 350 pF

The calculations have been done assuming that all power is delivered to the 200 V output voltage. Afterward, once the turn ratio has been defined, the transformer is designed to deliver the two output voltages, using the correct number of turns and the proper wire section.

The results of the 10 step procedure are summarized in *Table 1*:

Table 1. Design results

| Step	Parameter
1	$n = 0.975$
2	$M_{max} = 1.22$ $M_{min} = 0.93$
3	$f_{n.max} = 1.25$
4	$R_{ac} = 77.05\ \Omega$
5	$\lambda = 0.21$
6	$Q_{zvs.1} = 0.41$
7	$Q_{zvs.2} = 1.01$
8	$Q_{zvs} = 0.41$
9	$f_{min} = 80.6\ \text{kHz}$
10	$Z_o = 31.95\ \Omega\ \ C_r = 41.51\ \text{nF}$ $L_r = 42\ \mu H\ \ L_m = 197\ \mu H$

The chosen standard value of the resonant capacitor is 47 nF. The transformer has been designed using a two slot coil former and integrating both the series inductance L_r and the shunt inductance L_m, in order to obtain a magnetic component with the following parameters:

- $L_{p(SO)} = L_r + L_m = 240~\mu H$ primary inductance (with secondary windings open)

- $L_{p(SS)} = L_r = 40~\mu H$ primary inductance with secondary windings shorted

- $n_t = n \bullet \sqrt{1 + \lambda} = 1.08$ transformer turn ratio

The number of primary turns has been found experimentally, by measuring the "specific leakage inductance" (i.e. the leakage inductance per square turns) of a few suitable ferrite cores, using a two slot winding configuration. The procedure consists of winding a few layers of turns on both slots of the coil former (same copper area for primary and secondary) and then measuring the inductance of one winding with the other one short-circuited. Dividing this measured value by the squared number of turns gives the specific leakage inductance of the core - coil former construction. The chosen ferrite core is a ER-49-27-17 type, material grade PC44, and the necessary number of primary turns to obtain the required leakage inductance is 19. Therefore, the total number of secondary turns for 200 V output is 18 (from the required turn ratio n_t).

The secondary side of the transformer consists of two center tap windings, one for each output, and the two output voltages (+75 V and +200 V) are obtained by series connecting the two secondary windings on the DC side (refer to the electrical schematic in *Figure 12* for better understanding of circuit configuration). The bottom winding (for +75 V output) has 7 turns, while the top winding consists of 11 (18 - 7) turns.

Figure 12. LLC resonant half-bridge converter electrical schematic
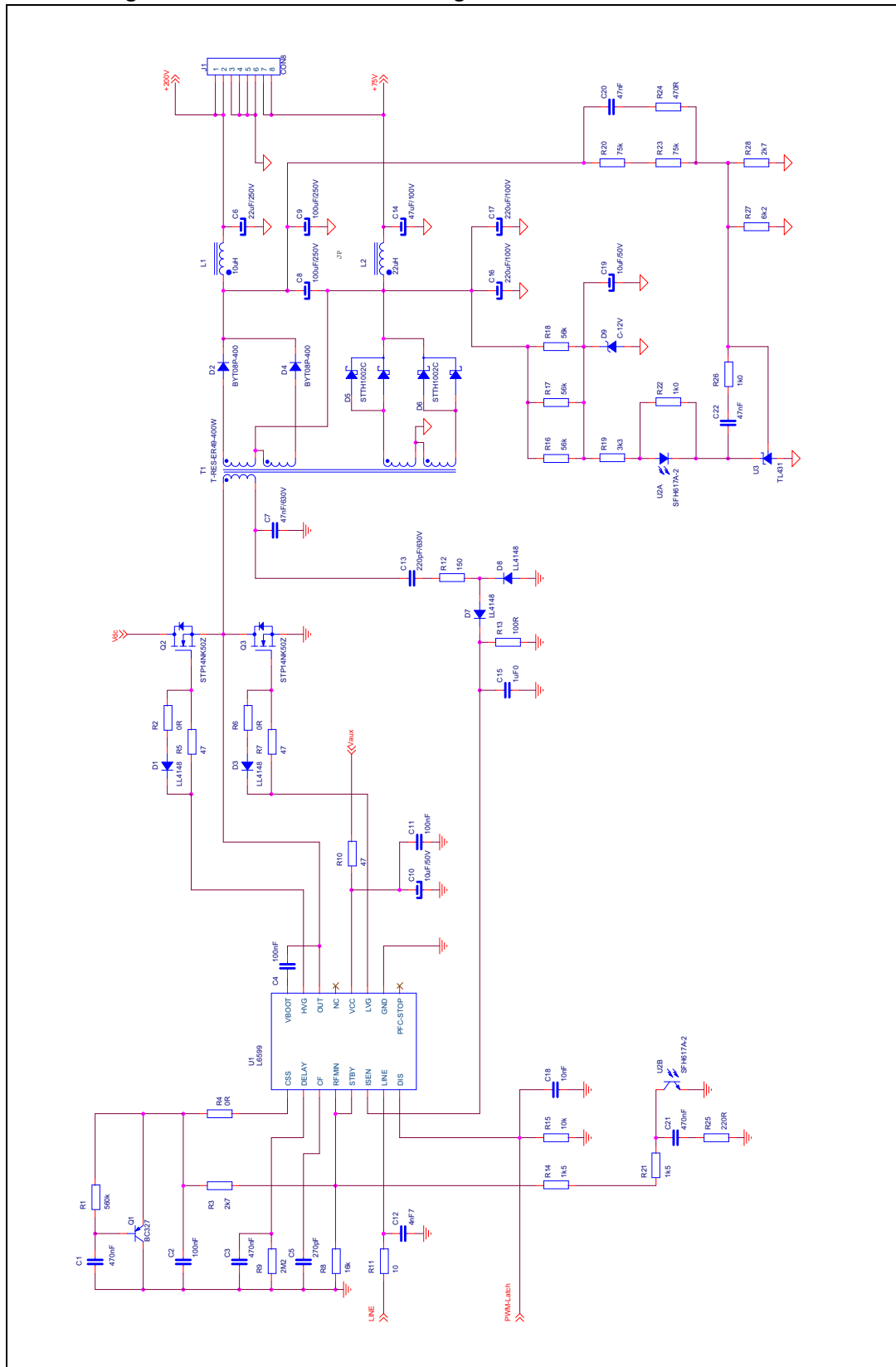
8 Electrical test results

8.1 Efficiency measurements

Table 2, *Table 3* and *Table 4* show the output voltage and current measurements at the various dc input voltage (nominal 390 Vdc, min 360 Vdc and max 420 Vdc) and several load conditions. For all measurements, both at full load and at light load operation, the input power has been measured by a digital power meter (Yokogawa WT-210). Particular attention has to be paid when measuring input power at full load in order to avoid measurement errors due to the voltage drop on cables and connections (connecting the WT-210 voltmeter termination to the board input connector). For the same reason, the measurements of the output voltages have been taken directly at the output connector, by using the remote sense option of the active load (Chroma 63108 and 63103) connected to the outputs.

Table 2. Efficiency measurements at V_{in} = 390 V_{dc}

+200 V	At load (A)	+75 (V)	At load (A)	P_{out} (W)	P_{in} (W)	Efficiency %
198.76	1.603	76.74	1.010	396.12	408.80	96.90%
198.75	1.300	76.80	0.811	320.66	330.81	96.93%
198.76	1.001	76.87	0.613	246.08	253.90	96.92%
198.79	0.751	76.95	0.414	181.15	187.54	96.59%
198.84	0.500	77.03	0.200	114.83	120.24	95.50%
198.87	0.151	77.06	0.107	38.27	42.70	89.64%

Table 3. Efficiency measurements at V_{in} = 360 V_{dc}

+200 V	At load (A)	+75 (V)	At load (A)	P_{out} (W)	P_{in} (W)	Efficiency %
198.68	1.603	76.68	1.010	395.93	409.47	96.69%
198.64	1.301	76.74	0.811	320.67	331.26	96.80%
198.62	1.000	76.81	0.613	245.70	254.17	96.67%
198.60	0.751	76.88	0.414	180.98	187.23	96.66%
198.57	0.500	76.94	0.198	114.52	120.43	95.09%
198.57	0.151	76.94	0.107	38.22	43.20	88.46%

Table 4. Efficiency measurements at $V_{in} = 420V_{dc}$

+200 V	At load (A)	+75 (V)	At load (A)	P_{out} (W)	P_{in} (W)	Efficiency %
198.35	1.601	76.57	1.008	394.74	407.45	96.88%
198.20	1.301	76.55	0.808	319.71	329.70	96.97%
197.87	1.001	76.47	0.609	244.64	252.55	96.87%
196.85	0.750	76.20	0.410	178.88	185.13	96.62%
198.01	0.504	76.74	0.198	114.99	119.78	96.00%
198.67	0.151	76.98	0.107	38.24	41.92	91.21%

The measurements have been done after 30 minutes of warm-up at maximum load. The circuit efficiency has been calculated at each load condition and input dc voltage and is plotted in *Figure 13*, showing very high values at maximum load level, higher than 96.5%. Also at light load, at an output power of about 10% of the maximum level, the converter efficiency is very good, reaching a value better than 88% in the whole DC input voltage range.

Figure 13. Circuit efficiency versus output power at various input voltages
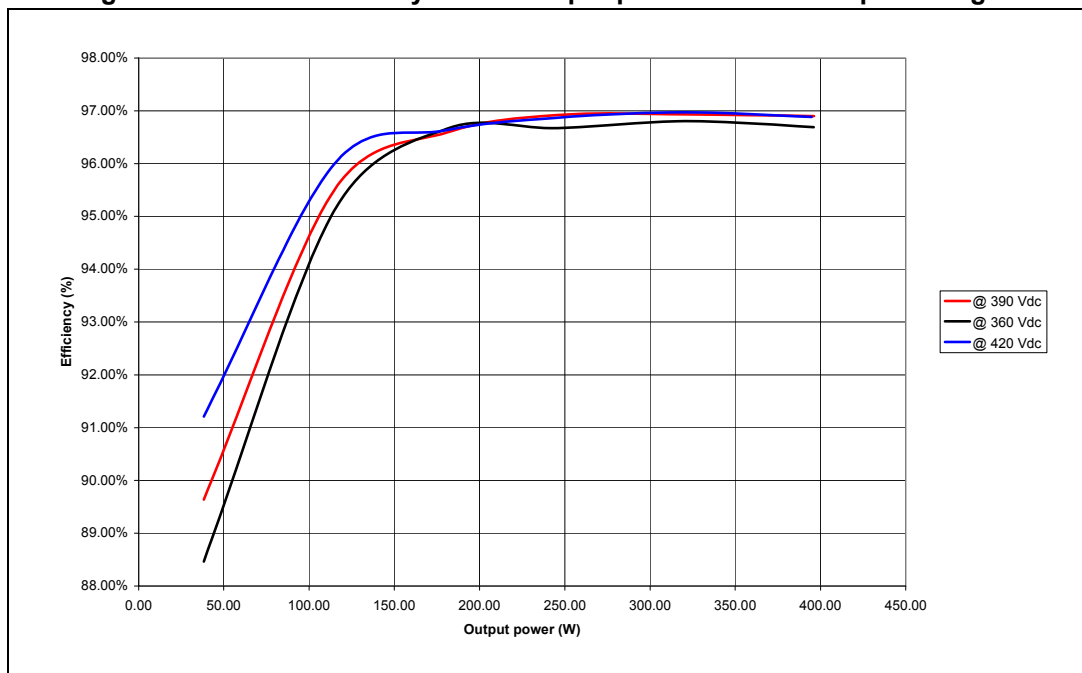
8.2 Resonant stage operating waveforms

Figure 14 shows some waveforms during steady state operation of the resonant circuit at nominal dc input voltage and full load. The Ch1 waveform is the half-bridge square voltage on pin 14 of the L6599, driving the resonant circuit. The trace Ch2 represents the transformer primary current flowing into the resonant tank. As shown, it is almost sinusoidal, because the operating frequency (about 123 kHz) is close to the resonance of the leakage inductance of the transformer and the resonant capacitor (C6). In this condition the circuit

has a good margin for ZVS operation, providing good efficiency, while the almost sinusoidal current waveform just allows for an extremely low EMI generation.

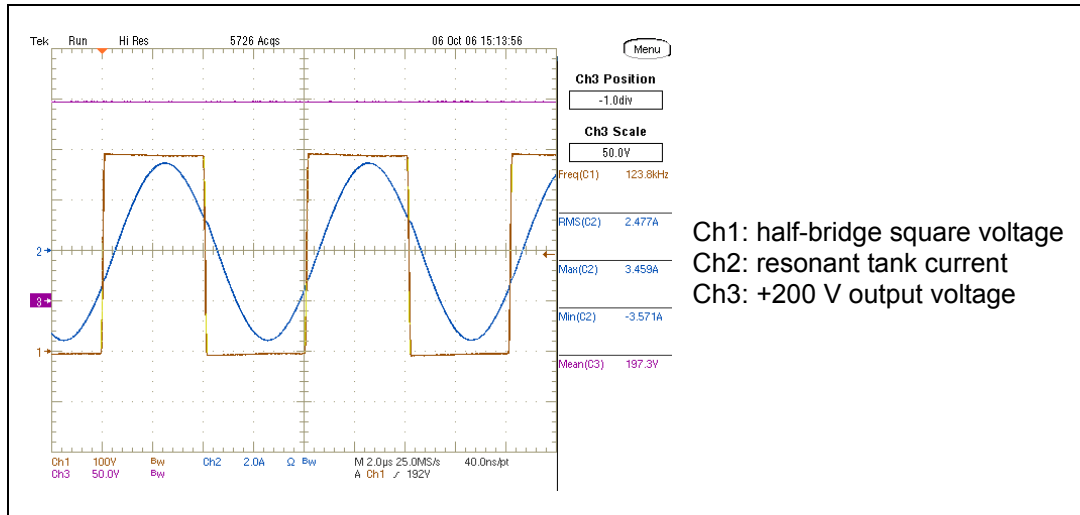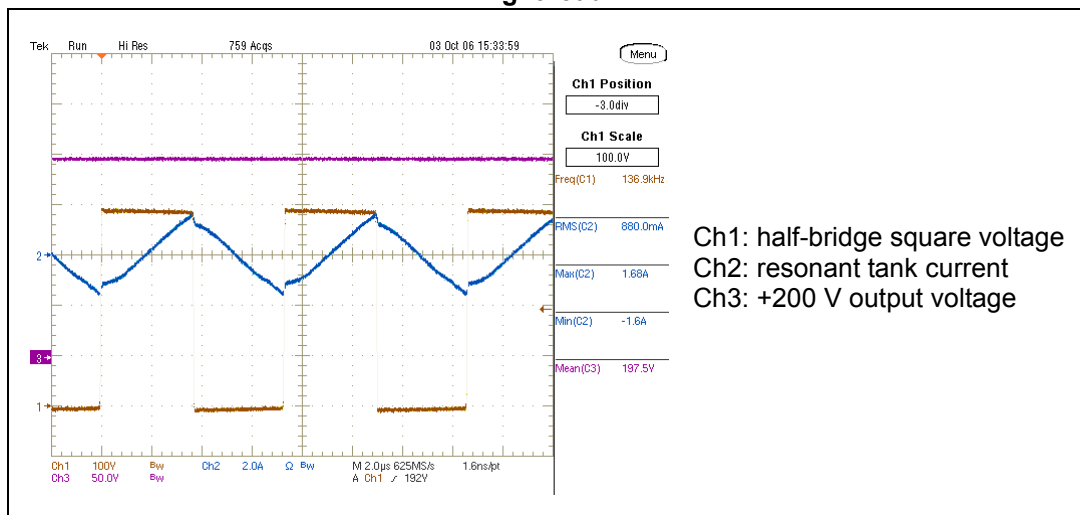**Figure 14. Resonant circuit primary side waveforms at nominal dc input voltage and full load**

Ch1: half-bridge square voltage
Ch2: resonant tank current
Ch3: +200 V output voltage

Figure 15 and *Figure 16* show the same waveforms as *Figure 14* with both outputs lightly loaded (50 mA each) and not loaded, respectively. These graphs demonstrate the ability of the converter to operate down to zero load, with the output voltages still within regulation limits (as can be seen looking at Ch3 waveform, representing the +200 V output voltage). The resonant tank current, in this load condition, assumes, obviously, an almost triangular shape and represents the magnetizing current flowing into the transformer primary side.

Figure 15. Resonant circuit primary side waveforms at nominal dc input voltage and light load

Ch1: half-bridge square voltage
Ch2: resonant tank current
Ch3: +200 V output voltage

Figure 16. Resonant circuit primary side waveforms at nominal dc input voltage and no-load

Ch1: half-bridge square voltage
Ch2: resonant tank current
Ch3: +200 V output voltage
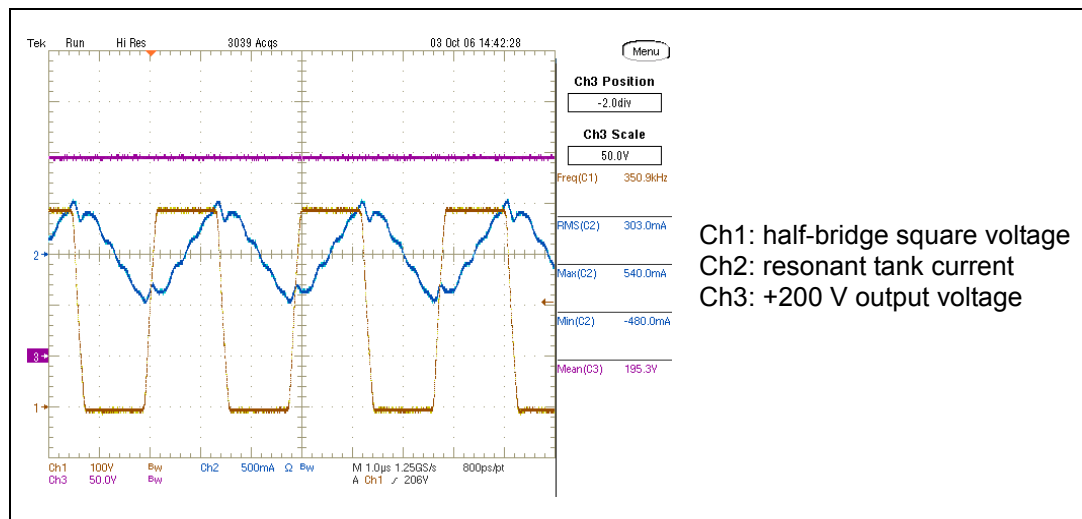
In *Figure 17*, the Ch1 waveform shows a detail of the half-bridge square voltage (directly taken across pin 14 and pin 10 of L6599 controller) to highlight the softness of voltage edge, without abrupt negative voltage spikes that would be generated in presence of large stray inductance of wiring. The layout is very critical in this respect and needs to be optimized in order to minimize this effect, which could damage the controller itself.

In *Figure 18* and *Figure 19*, waveforms relevant to the secondary side are represented. The rectifiers reverse voltage is measured by CH1 (for both +200 V and +75 V outputs) and the peak-to-peak value is indicated on the right of the graph. Waveform CH2 shows the current flowing into one of the two output diodes for each output voltage (respectively D6 and D8). Also this current shape is almost a sine wave, whose average value is one half the output current.

Figure 17. Resonant circuit primary side waveforms at nominal dc input voltage and light load
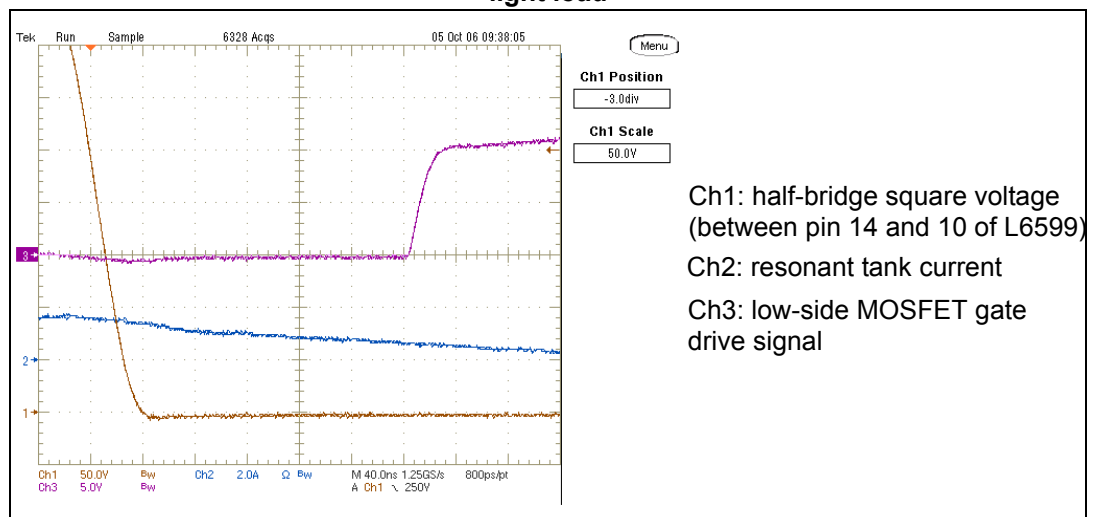

Ch1: half-bridge square voltage (between pin 14 and 10 of L6599)

Ch2: resonant tank current

Ch3: low-side MOSFET gate drive signal

Figure 18. +200 V output diode voltage and current waveforms

+200 V output waveforms:
Ch1: +200 V diode reverse voltage
Ch2: diode D6 current
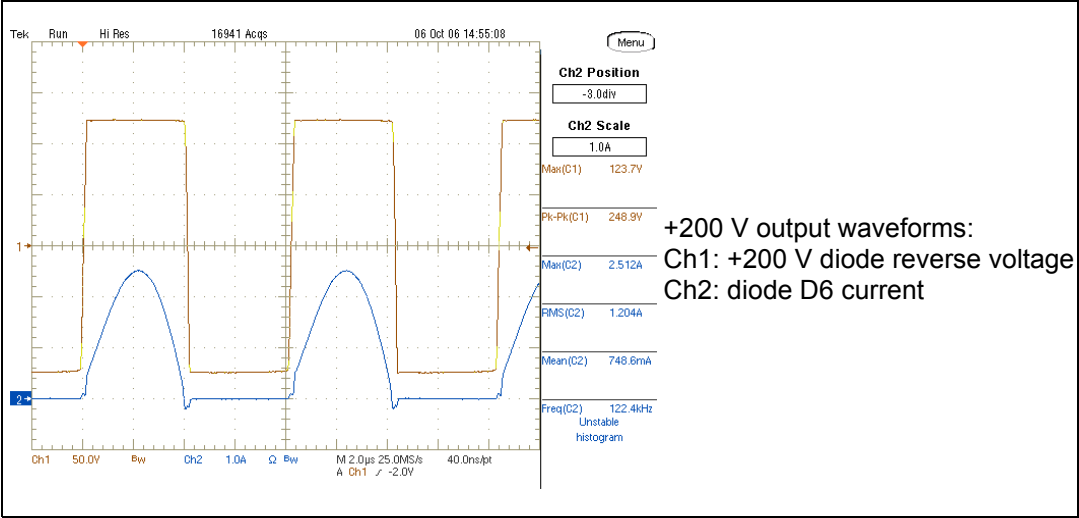
Figure 19. +75 V output diode voltage and current waveforms

+75 V output waveforms:
Ch1: resonant tank current
Ch2: diode D8 current
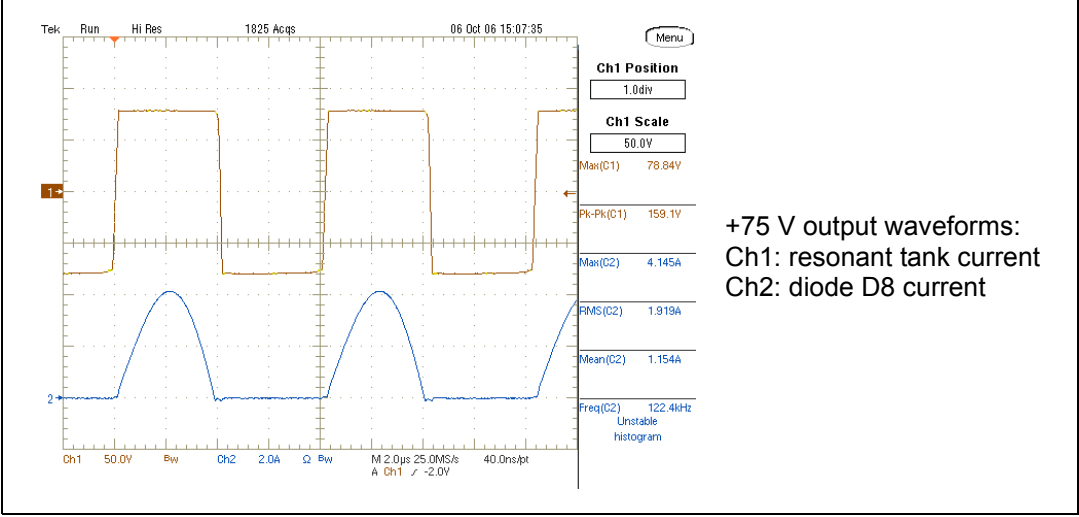
9 Reference

1. Steady-state Analysis of the LLC Resonant Converter, Applied Power Electronics Conference and Exposition, 2001. APEC 2001. Pages: 728 - 735

2. A Comparison of Half Bridge Resonant Converter Topologies, IEEE Trans. on Power Electronics, 1988. Pages: 174 - 182.

3. First harmonic approximation including design constraints, Telecommunications Energy Conference, 1998. INTELEC. Pages: 321 - 328

4. Design Optimization for an LCL-Type Series Resonant Converter, see www.powerpulse.net.

5. L6599 High-voltage resonant controller datasheet, STMicroelectronics

10 Revision history

Table 5. Document revision history

Date	Revision	Changes
11-Jan-2007	1	First issue
06-Mar-2007	2	Minor text change
26-Mar-2007	3	*Equation 53* modified
24-Jul-2007	4	Quality factor (Q) modified
25-Oct-2007	5	Modified: *Equation 14* and *Equation 33*
17-Mar-2014	6	Updated *Equation 31 on page 13* (added "^{2}" to "$\|H_{LOSS}(j\omega)\|$"). Updated cross-references throughout document. Minor modifications throughout document.

Please Read Carefully:

Information in this document is provided solely in connection with ST products. STMicroelectronics NV and its subsidiaries ("ST") reserve the right to make changes, corrections, modifications or improvements, to this document, and the products and services described herein at any time, without notice.

All ST products are sold pursuant to ST's terms and conditions of sale.

Purchasers are solely responsible for the choice, selection and use of the ST products and services described herein, and ST assumes no liability whatsoever relating to the choice, selection or use of the ST products and services described herein.

No license, express or implied, by estoppel or otherwise, to any intellectual property rights is granted under this document. If any part of this document refers to any third party products or services it shall not be deemed a license grant by ST for the use of such third party products or services, or any intellectual property contained therein or considered as a warranty covering the use in any manner whatsoever of such third party products or services or any intellectual property contained therein.

UNLESS OTHERWISE SET FORTH IN ST'S TERMS AND CONDITIONS OF SALE ST DISCLAIMS ANY EXPRESS OR IMPLIED WARRANTY WITH RESPECT TO THE USE AND/OR SALE OF ST PRODUCTS INCLUDING WITHOUT LIMITATION IMPLIED WARRANTIES OF MERCHANTABILITY, FITNESS FOR A PARTICULAR PURPOSE (AND THEIR EQUIVALENTS UNDER THE LAWS OF ANY JURISDICTION), OR INFRINGEMENT OF ANY PATENT, COPYRIGHT OR OTHER INTELLECTUAL PROPERTY RIGHT.

ST PRODUCTS ARE NOT DESIGNED OR AUTHORIZED FOR USE IN: (A) SAFETY CRITICAL APPLICATIONS SUCH AS LIFE SUPPORTING, ACTIVE IMPLANTED DEVICES OR SYSTEMS WITH PRODUCT FUNCTIONAL SAFETY REQUIREMENTS; (B) AERONAUTIC APPLICATIONS; (C) AUTOMOTIVE APPLICATIONS OR ENVIRONMENTS, AND/OR (D) AEROSPACE APPLICATIONS OR ENVIRONMENTS. WHERE ST PRODUCTS ARE NOT DESIGNED FOR SUCH USE, THE PURCHASER SHALL USE PRODUCTS AT PURCHASER'S SOLE RISK, EVEN IF ST HAS BEEN INFORMED IN WRITING OF SUCH USAGE, UNLESS A PRODUCT IS EXPRESSLY DESIGNATED BY ST AS BEING INTENDED FOR "AUTOMOTIVE, AUTOMOTIVE SAFETY OR MEDICAL" INDUSTRY DOMAINS ACCORDING TO ST PRODUCT DESIGN SPECIFICATIONS. PRODUCTS FORMALLY ESCC, QML OR JAN QUALIFIED ARE DEEMED SUITABLE FOR USE IN AEROSPACE BY THE CORRESPONDING GOVERNMENTAL AGENCY.

Resale of ST products with provisions different from the statements and/or technical features set forth in this document shall immediately void any warranty granted by ST for the ST product or service described herein and shall not create or extend in any manner whatsoever, any liability of ST.

STMicroelectronics group of companies

Australia - Belgium - Brazil - Canada - China - Czech Republic - Finland - France - Germany - Hong Kong - India - Israel - Italy - Japan - Malaysia - Malta - Morocco - Philippines - Singapore - Spain - Sweden - Switzerland - United Kingdom - United States of America

www.st.com